Diverse innate immune factors protect yeast from lethal viral pathogenesis

Sabrina Chau[1], Jie Gao[1], Annette J. Diao[1], Shi Bo Cao[1], Alan R. Davidson[1,2], and Marc D. Meneghini[1*]
[1]Department of Molecular Genetics, University of Toronto, 661 University Ave, Toronto, ON, M5G 1M1, Canada.
[2]Department of Biochemistry, University of Toronto, 661 University Ave, Toronto, ON, M5G 1M1, Canada.

[*]Correspondence: marc.meneghini@utoronto.ca

Summary

In recent years, newly characterized antiviral systems have been found to be remarkably conserved from bacteria to mammals, revealing the potential to gain unique insight into these systems through the study of microbial organisms[1]. Despite the enthusiasm generated by these findings, the key microbial model organism *Saccharomyces cerevisiae* (budding yeast) has been minimally exploited for studies of viral defense, primarily because it is not infected with exogenously transmitted viruses. However, most yeast strains are infected with an endogenous double stranded RNA (dsRNA) virus called L-A, and previous studies have identified conserved antiviral systems that attenuate L-A replication[2]. Although these systems do not lead to eradication of L-A, we show here that they collaboratively prevent massive over-proliferation of L-A that leads to proteostatic stress and lethality. Exploiting this new insight, we asked if the powerful genetic screening methods available in yeast could be used to identify additional conserved antiviral systems. Validating this approach, we discovered antiviral functions for the yeast homologs of polyA-binding protein (PABPC1) and the La-domain containing protein Larp1, which are both involved in viral innate immunity in humans[3,4]. We also identify new antiviral functions for the RNA exonucleases *REX2* and *MYG1*, both of which have distinct but poorly characterized human and bacterial homologs[5-8]. These findings highlight the potential of yeast as a powerful model system for studies of the ubiquitous host-virus arms race.

Results and discussion

L-A belongs to the broadly dispersed *Totiviridae* family of double stranded RNA (dsRNA) viruses, which has no extracellular phase and is transmitted vertically through cell division or fusion[2]. L-A transcripts encode the capsid (Gag) proteins that comprise most of its viral particle as well as a Gag-pol fusion protein produced at much lower levels that provides RNA dependent RNA polymerase activity

34 responsible for replication and transcription. Encapsidation of viral transcripts within nascent particles
35 completes the L-A lifecycle[2]. L-A replication is maintained at a low level through the activities of the
36 *SKI2*, *3*, and *8* genes, which encode subunits of a conserved ribosome-associated complex that opposes
37 the translation of transcripts such as those encoded by L-A that lack polyA tails[9-11]. A separate pathway
38 of L-A attenuation is provided by Xrn1, a 5'-3' exoribonuclease that degrades uncapped mRNAs[12,13].
39 Both of these systems have been associated with antiviral defense in mammals[14-17].
40 We showed that L-A was held in check during sporulation by the mitochondrial DNA/RNA
41 endonuclease Nuc1, a homolog of endonuclease G (EndoG) found in all eukaryotes and many
42 prokaryotes[18]. EndoG is involved in mammalian programmed cell death that frequently occurs in virus
43 infected cells, and programmed cell death is intrinsic to yeast sporulation[19-22]. These and other
44 observations have led to speculation that Nuc1/EndoG may reflect a prokaryotic antiviral origin of
45 programmed cell death[23]. To query *NUC1* anti-viral function outside of sporulation and its associated
46 programmed cell death, we investigated L-A attenuation in mitotic haploid cells in the reference
47 BY4742 strain background. Visualization of L-A dsRNA using ethidium bromide staining of
48 electrophoresed RNA revealed that while *nuc1*Δ and *ski3*Δ single mutants exhibited no effect,
49 combining *nuc1*Δ and *ski3*Δ led to a large increase in L-A dsRNA **(Fig 1A)**. We corroborated these
50 findings using immunofluorescence microscopy with a dsRNA antibody widely used to detect
51 replicating RNA viruses[24,25]. These images revealed L-A dsRNA to accumulate in foci, reminiscent of
52 "viral factory" sites of viral replication observed in human cells **(Fig 1B and S1)**[26]. Consistent with
53 previous findings in other strain backgrounds, western blotting showed that Gag protein levels were
54 elevated in *nuc1*Δ and *ski3*Δ mutants[12,18,27], and we determined that *nuc1*Δ *ski3*Δ double mutants
55 accumulated massively elevated Gag levels, confirming that *NUC1* and *SKI3* participate in separate
56 antiviral pathways **(Fig 2A)**.
57 We used spot test growth assays to determine if high L-A viral load had any fitness consequence
58 and found that *nuc1*Δ *ski3*Δ double mutants grew normally at 30˚ C but exhibited conditional lethality at
59 37˚ C **(Fig 2B)**. Modest growth defects of *nuc1*Δ and *ski3*Δ single mutants were observed at high
60 temperature when cells were grown with glycerol rather than glucose as the carbon source, a condition
61 under which yeast relies on mitochondrial respiration **(Fig 2B)**. These growth phenotypes were
62 completely reversed in isogenic strains cured of L-A (L-A^0), implying that unrestricted L-A replication
63 caused them (**Fig 2B**).
64 As expected, a *NUC1*-expressing plasmid restored viability to a *nuc1*Δ *ski3*Δ strain grown at high
65 temperature and elicited a corresponding decrease in Gag levels (**Fig 2A and 2B**). We observed similar
66 suppression of *nuc1*Δ *ski3*Δ using plasmid driven *XRN1* over-expression, suggesting that Xrn1 repressed

67 L-A via a parallel mechanism **(Fig 2A and 2B)**. Consistent with this model, *nuc1*Δ *xrn1*Δ mutants
68 accumulated greatly elevated levels of Gag and exhibited L-A-dependent conditional lethality at high
69 temperature **(Fig S2A and S2B)**, and *xrn1*Δ *ski3*Δ mutants are inviable[28]. We conclude that Nuc1, Ski3
70 and Xrn1 convergently oppose L-A, and that L-A causes lethal pathogenesis at high temperature when
71 unattenuated **(Fig 2C)**.
72 Since *XRN1* over-expression suppressed the growth defects of a *nuc1*Δ *ski3*Δ strain, we
73 hypothesized that over-expression of other antiviral factors would produce a similar effect, and that this
74 phenomenon could be used as a screen to identify new antiviral systems. To test this idea, we employed
75 a high-copy plasmid suppression screen to detect genes whose overexpression alleviated the conditional
76 lethality of *nuc1Δ ski3Δ*. Using this strategy, we identified *SRO9*, *SLF1*, and *PAB1* as high-copy
77 suppressors, all of which encode ribosome-associated RNA binding proteins **(Fig 3A)**[29,30]. Sro9 and Slf1
78 are paralogous lupus-autoantigen (La) domain containing proteins broadly found in eukaryotes.
79 Interestingly, the human Sro9/Slf1 ortholog Larp1 was recently found to bind to SARS-Cov-2 plus-
80 strand ssRNA and to oppose its replication in human cells through an unknown mechanism[3]. *PAB1*
81 encodes the highly conserved PolyA-Binding Protein (PABPC1 in humans), which is a common target
82 of viral inhibition through diverse mechanisms[4]. *PAB1* and *SRO9* overexpression markedly reduced Gag
83 levels, explaining their rescuing phenotypes **(Fig 3B)**. Curiously, even though *SLF1* overexpression
84 rescued the *nuc1*Δ *ski3*Δ growth defect just as well as *SRO9*, it did not lead to any reduction in Gag
85 levels **(Fig 3A and 3B)**. These findings suggest that *SRO9* rescues cells by opposing L-A replication and
86 that *SLF1* protects cells from the pathogenic consequences of elevated viral replication **(Fig 2C)**.
87 To gain insight into the divergent mechanisms of Sro9 and Slf1, we considered further what
88 physiological consequences L-A pathogenesis has and how *SRO9*/*SLF1* might differentially impact
89 them. We noted a previous study in which deletions of *NUC1* or of *SKI*-complex genes led to weak
90 induction of a proteostatic stress GFP reporter gene controlled by Hsf1, a conserved transcription factor
91 that senses proteostatic stress and activates the gene expression response[31-34]. Using flow cytometry with
92 this reporter (HSE-GFP), we determined that a *nuc1*Δ *ski3*Δ double mutant exhibited strong activation of
93 HSE-GFP and that this activation was reverted in L-A^0 strains **(Fig 3C and S3)**. We hypothesized that
94 the massive accumulation of Gag observed in *nuc1*Δ *ski3*Δ mutants accounted for this proteostatic stress
95 response. Supporting this, HSE-GFP activation of a *nuc1*Δ *ski3*Δ double mutant was reverted by *PAB1*
96 or *SRO9* over-expression, but not by *SLF1* over-expression, mirroring these genes respective
97 consequences for Gag accumulation **(Fig 3B and 3C)**. The evolutionary divergence of *SRO9* and *SLF1*
98 has thus resulted in different viral-protective mechanisms, with *SRO9* opposing viral protein
99 accumulation and associated proteostatic stress, and *SLF1* possibly protecting cells from the toxic

100 consequences of viral induced proteostatic stress **(Fig 2C)**.

101 To identify new antiviral factors using a different approach, we searched a curated genetic
102 interaction database for gene deletions that caused a synergistic growth defect when combined with
103 *nuc1Δ* in at least two high-throughput screening studies. We found twenty-one such examples[35], two of
104 which we confirmed as new viral attenuation factors. The first of these, *REX2*, is conserved from
105 bacteria to humans[5]. Both Rex2 and its human homolog REXO2 are mitochondrial-localized 3'-5' RNA
106 exonucleases that contain an EXOIII domain widely found in prokaryotic and eukaryotic proteins,
107 including the interferon stimulated antiviral protein ISG20[6,7,36-38]. Mutant strains combining *rex2*Δ with
108 *nuc1*Δ accumulated greatly increased levels of Gag and exhibited L-A-dependent lethality at high
109 temperature **(Fig 4A and 4B)**. Remarkably, *nuc1*Δ *ski3*Δ *rex2*Δ and *nuc1*Δ *xrn1*Δ *rex2*Δ triple mutants
110 were inviable under all growth conditions and these defects were reversed in L-A^0 strains **(Fig S4)**.
111 These findings demonstrate the severe pathogenic potential of L-A and identify a new and highly
112 conserved mitochondrial localized antiviral RNA nuclease **(Fig 2C)**.

113 The second gene identified in our survey was *MYG1*, the yeast homolog of human MelanocYte
114 proliferation Gene 1, a 3'-5' RNA exonuclease associated with the human auto-immune disorder
115 vitiligo[8,39]. Phylogenetic analysis has identified *MYG1* orthologs across all taxa[8]. A *myg1*Δ *nuc1*Δ
116 double mutant strain displayed large increases of Gag accumulation compared to the single mutants and
117 exhibited L-A-dependent lethality at high temperature **(Fig 4C, 4D, and S5)**. We were able to recover
118 *nuc1*Δ *ski3*Δ *myg1*Δ triple mutants, though they were extremely slow growing at 30˚ C and accumulated
119 even higher levels of Gag **(Fig 4C and 4D)**. These growth defects were also completely reversed in L-
120 A^0 strains **(Fig S5)**. *MYG1* thus represents a new viral attenuation factor, acting in parallel to both *NUC1*
121 and the *SKI* complex **(Fig 2C)**. Reflecting its underpinning as an auto-immune disease, Vitiligo is
122 triggered by viral infection and is associated with mutations in the intracellular viral sensor MDA5[40]. An
123 interesting possibility our findings thus suggest is that the elevated h*MYG1* expression associated with
124 vitiligo may reflect an antiviral role for this protein[39]. Indeed, growth defects caused by *myg1*Δ are
125 complemented by human Myg1, demonstrating a functional conservation to further investigate[8].

126 Although insightful studies of the L-A virus have been carried out, the L-A virus system has not
127 yet been extensively exploited as a model for studying viral innate immunity, owing largely to its
128 apparent benign nature. Here, we show that L-A is profoundly consequential for yeast fitness when its
129 replication is uncontrolled, and that diverse innate immune pathways contribute to maintaining L-A
130 replication at a harmless level. Importantly, our discovery that L-A is attenuated by homologs of known
131 human antiviral factors (*SRO9*/*SLF1* and *PAB1*) supports the hypothesis that *REX2* and *MYG1* homologs
132 may have viral innate immune functions in other organisms. Of note, Rex2 expands the arsenal of

133 mitochondrial localized antiviral nucleases beyond Nuc1, suggesting a key role of mitochondria in yeast
134 viral attenuation. Among the many possible explanations for this, one scenario is that some aspect of the
135 L-A replication cycle occurs in physical association with mitochondria similarly to as documented for
136 the plus strand ssRNA flock house virus[41]. Whatever the case may be, our results highlight a potential
137 general importance of mitochondria for viral innate immunity in eukaryotes, and position the yeast-L-A
138 system as a powerful model for further studies of this topic[42].
139

140 **Acknowledgements**

141 We are grateful Dr. Charlie Boone and Dr. Brenda Andrews for generous sharing of strains and plasmid
142 and to Angus McQuibban for critical comments on the manuscript. M.D.M. is funded by NSERC
143 RGPIN-2019-07230. A.R.D. is funded by CIHR FDN-15427.
144

145 **Author Contributions**

146 S.C., J.G., A.D., S.B.C., and M.D.M. conceived, planned, and executed the experiments.
147 S.C., J.G., A.D., and M.D.M. analyzed the data. S.C., A.R.D., and M.D.M. wrote the manuscript.
148

149 **Declaration of interests**

150 We declare no competing financial interests.
151

152 **STAR Methods**

153 **Key Resources Table.**

REAGENT or RESOURCE	Source	Identifier
Antibodies		
HRP-conjugated horse anti-mouse	Cell Signaling Technology	Cat # 7075
HRP-conjugated goat anti-rabbit	Cell Signaling Technology	Cat # 7074
Anti-Pgk1	Abcam	Cat # ab113684
Anti-L-A Gag	Reed Wickner	
Anti-Sro9	Sandra Wolin	Sobel et al.[29]
Anti-Slf1	Sandra Wolin	Sobel et al.[29]
J2 anti-dsRNA	SCICONS	
Cyanine3 conjugated goat anti-mouse	Jackson ImmunoResearch Laboratories	
Experimental models: Organisms/strains*		
BY4741 *MAT*a L-A^0 *nuc1Δ::NatMX6 ski3Δ::HygMX6*	This study	jgy42
BY4741 *MAT*a L-A$^+$ p5476 *2μ LEU2*	This study	jgy156
BY4741 *MAT*a L-A$^+$ *nuc1Δ::NatMX6 ski3Δ::HygMX6* p5476 *2μ LEU2*	This study	jgy157

BY4741 *MAT*a L-A^{+} *nuc1Δ::NatMX6 ski3Δ::HygMX6* p5476 *PAB1 2μ LEU2*	This study	jgy158
BY4741 *MAT*a L-A^{+} *nuc1Δ::NatMX6 ski3Δ::HygMX6* p5476 *SRO9 2μ LEU2*	This study	jgy171
BY4741 *MAT*a L-A^{+} *nuc1Δ::NatMX6 ski3Δ::HygMX6* p5476 *SLF1 2μ LEU2*	This study	jgy173
BY4741 *MAT*α L-A^{+} *nuc1Δ::NatMX6*	This study	mmy4076
BY4741 *MAT*α L-A^{+}	This study	mmy4699
BY4741 *MAT*a L-A^{+}	This study	mmy6042
BY4741 *MAT*a L-A^{+} *ski3Δ::HygMX6*	This study	mmy6860
BY4741 *MAT*a L-A^{+}	This study	mmy7701
BY4741 *MAT*α L-A^{0}	This study	mmy8064
BY4741 *MAT*a L-A^{+} *nuc1Δ::NatMX6 ski3Δ::HygMX6*	This study	mmy8213
BY4741 *MAT*α L-A^{0}	This study	mmy8244
BY4741 *MAT*a L-A^{0}	This study	mmy8245
BY4741 *MAT*α L-A^{0} *nuc1Δ::NatMX6*	This study	mmy8246
BY4741 *MAT*a L-A^{0} *nuc1Δ::NatMX6*	This study	mmy8247
BY4741 *MAT*a L-A^{0} *nuc1Δ::NatMX6*	This study	mmy8466
BY4741 *MAT*α L-A^{+} *nuc1Δ::NatMX6 ski3Δ::HygMX6* p5476 *2μ LEU2*	This study	mmy9292
BY4741 *MAT*α L-A^{+} *nuc1Δ::NatMX6 ski3Δ::HygMX6* p5476 *NUC1 2μ LEU2*	This study	mmy9293
BY4741 *MAT*α L-A^{+} *nuc1Δ::NatMX6* p5476 *2μ LEU2*	This study	mmy9320
BY4741 *MAT*α L-A^{+} p5476 *2μ LEU2*	This study	mmy9321
BY4741 *MAT*α L-A^{0} *nuc1Δ::NatMX6 ski3Δ::HygMX6* p5476 *2μ LEU2*	This study	mmy9322
BY4741 *MAT*α L-A^{+} *ski3Δ::HygMX6* p5476 *2μ LEU2*	This study	mmy9323
BY4741 *MAT*a L-A^{+} *nuc1Δ::NatMX6 rex2Δ::KanMX6*	This study	mmy9342
BY4741 *MAT*a L-A^{+} *rex2Δ::KanMX6*	This study	mmy9344
BY4741 *MAT*α L-A^{+} *nuc1Δ::NatMX6 ski3Δ::HygMX6* p5476 *XRN1 2μ LEU2*	This study	mmy9350
BY4741 *MAT*α L-A^{+} *nuc1Δ::NatMX6 xrn1Δ::KanMX6*	This study	mmy9351
BY4741 *MAT*α L-A^{+} *xrn1Δ::KanMX6*	This study	mmy9353
BY4741 *MAT*α L-A^{0} *xrn1Δ::NatMX6*	This study	mmy9609
BY4741 *MAT*α L-A^{0} *xrn1Δ::NatMX6 nuc1Δ::HygMX6*	This study	mmy9611
BY4741 *MAT*a L-A^{+} *nuc1Δ::NatMX6 rex2Δ::HygMX6 xrn1Δ::KanMX6* pRS316 *NUC1-FLAG URA3*	This study	mmy10001
BY4741 *MAT*α L-A^{0} *xrn1Δ::NatMX6 nuc1Δ::HygMX6 rex2Δ::KanMX6* pRS316 *NUC1-FLAG URA3*	This study	mmy10003

BY4741 *MAT*α L-A^0 *URA3::HSE-EmGFP nuc1Δ::NatMX6 ski3Δ::HygMX6*	This study	mmy10007
BY4741 *MAT*α L-A$^+$ *URA3::HSE-EmGFP nuc1Δ::NatMX6*	This study	mmy10073
BY4741 *MAT*α L-A$^+$ *URA3::HSE-EmGFP nuc1Δ::NatMX6 ski3Δ::HygMX6*	This study	mmy10074
BY4741 *MAT*a L-A$^+$ *URA3::HSE-EmGFP ski3Δ::HygMX6*	This study	mmy10076
BY4741 *MAT*α L-A$^+$ *URA3::HSE-EmGFP*	This study	mmy10077
BY4741 *MAT*a L-A$^+$ *nuc1Δ::NatMX6 ski3Δ::HygMX6* p5476 *2μ LEU2*	This study	mmy10461
BY4741 *MAT*a L-A$^+$ *nuc1Δ::NatMX6 ski3Δ::HygMX6* p5476 *SRO9 2μ LEU2*	This study	mmy10462
BY4741 *MAT*a L-A$^+$ *nuc1Δ::NatMX6 ski3Δ::HygMX6* p5476 *SLF1 2μ LEU2*	This study	mmy10463
BY4741 *MAT*a L-A$^+$ *nuc1Δ::NatMX6 ski3Δ::HygMX6* p5476 *PAB1 2μ LEU2*	This study	mmy10464
BY4741 *MAT*α L-A$^+$ *nuc1Δ::NatMX6 myg1Δ::KanMX6*	This study	mmy10845
BY4741 *MAT*a L-A$^+$ *ski3Δ::HygMX6 myg1Δ::KanMX6*	This study	mmy10846
BY4741 *MAT*α L-A$^+$ *myg1Δ::KanMX6*	This study	mmy10847
BY4741 *MAT*α L-A^0 *nuc1Δ::NatMX6 ski3Δ::HygMX6 myg1Δ::KanMX6*	This study	mmy10848
BY4741 *MAT*a L-A^0 *nuc1Δ::NatMX6 myg1Δ::KanMX6*	This study	mmy10849
BY4741 *MAT*α L-A$^+$ *nuc1Δ::NatMX6 ski3Δ::HygMX6 myg1Δ::KanMX6*	This study	mmy10852
BY4741 *MAT*a L-A^0 *rex2Δ::KanMX6*	This study	scy629
BY4741 *MAT*a L-A^0 *nuc1Δ::NatMX6 rex2Δ::KanMX6*	This study	scy630
BY4741 *MAT*a L-A$^+$ *nuc1Δ::NatMX6 ski3Δ::HygMX6 rex2Δ::KanMX6* pRS316 *NUC1 URA3*	This study	scy633
BY4741 *MAT*a L-A^0 *nuc1Δ::NatMX6 ski3Δ::HygMX6 rex2Δ::KanMX6* pRS316 *NUC1 URA3*	This study	scy635
BY4741 *MAT*a L-A$^+$ L-BC^0 *nuc1Δ::NatMX6 ski3Δ::HygMX6*	This study	scy838
BY4741 *MAT*a L-A$^+$ L-BC^0	This study	scy839
BY4741 *MAT*a L-A$^+$ L-BC^0 *ski3Δ::HygMX6*	This study	scy841
BY4741 *MAT*a L-A$^+$ L-BC^0 *nuc1Δ::NatMX6*	This study	scy842
BY4741 *MAT*a L-A^0 L-BC^0 *nuc1Δ::NatMX6 ski3Δ::HygMX6*	This study	scy894
BY4741 *MAT*a L-A$^+$ *URA3::HSE-EmGFP* p5476 *2μ LEU2*	This study	scy1100

BY4741 *MAT*α L-A$^+$ *URA3::HSE-EmGFP nuc1Δ::NatMX6 ski3Δ::HygMX6* p5476 *2μ LEU2*	This study	scy1104
BY4741 *MAT*α L-A$^+$ *URA3::HSE-EmGFP nuc1Δ::NatMX6 ski3Δ::HygMX6* p5476 *PAB1 2μ LEU2*	This study	scy1105
BY4741 *MAT*α L-A$^+$ *URA3::HSE-EmGFP nuc1Δ::NatMX6 ski3Δ::HygMX6* p5476 *SLF1 2μ LEU2*	This study	scy1106
BY4741 *MAT*α L-A$^+$ *URA3::HSE-EmGFP nuc1Δ::NatMX6 ski3Δ::HygMX6* p5476 *SRO9 2μ LEU2*	This study	scy1107
Software and algorithms		
ImageJ	N/A	https://imagej.nih.gov/ij/
Volocity	Volocity	https://www.volocity4d.com/
Flowing	Turku Bioscience	https://bioscience.fi/
Excel	Microsoft	https://www.microsoft.com/
R studio	Rstudio	https://www.rstudio.com/

*Strain background
BY4741 *his3 ura3 leu2*

Lead Contact and Materials Availability.

Further information and requests for yeast strains, resources, and reagents should be directed to and will be fulfilled by the lead contact, Marc Meneghini (marc.meneghini@utoronto.ca).

Experimental Model and Subject Details.

Strains were grown at 30°C in either YPAD or synthetic complete media with appropriate amino acid drop out for plasmid maintenance unless otherwise specified.

Method Details.

Strains, media, and plasmids.

Standard *S. cerevisiae* genetic and strain manipulation techniques were used for strain construction. Refer to STAR Methods for strains and plasmids used in this paper. The yOB255 *URA3::HSE-EmGFP* strain was obtained from Onn Brandman[43]. The p5476 *2μ LEU2*, p5476 *NUC1 2μ LEU2*, p5476 *XRN1 2μ LEU2*, p5476 *PAB1 2μ LEU2*, p5476 *SRO9 2μ LEU2*, p5476 *SLF1 2μ LEU2* MOBY plasmids were

171 obtained from Brenda Andrews[44]. The pVB3011 *L-BC GAG (P_{GAL1})* plasmid was obtained from
172 Suzanne Sandmeyer[45].
173
174 **Spot analysis.**
175 Yeast strains were grown overnight at 30°C to saturation. Each strain was diluted to an OD_{600} = 0.4,
176 serial diluted four times by 10-fold, and spotted onto agar plates containing synthetic complete media or
177 drop out media supplemented with the indicated carbon source (2% glucose or 3% glycerol).
178
179 **Protein extraction and Western blot.**
180 5 OD of log-phase cells were harvested and permeabilized with 0.1N NaOH at room temperature for 5
181 minutes. The cells were then pelleted and resuspended in SDS/PAGE buffer before heating at 100°C for
182 10 minutes. The samples were centrifuged to isolate the soluble fraction for Western blotting. Protein
183 concentrations were determined with an RC/DC assay (BioRad 5000121). Equal amounts of protein
184 were electrophoresed on 10% SDS/PAGE and transferred to poly(vinylidene difluoride) membranes.
185 Blots were incubated in primary antibody overnight and probed with 1:3,000 horseradish peroxidase
186 (HRP)-conjugated horse anti-mouse (7075; Cell Signaling Technology) or goat anti-rabbit (7074; Cell
187 Signaling Technology) secondary antibody. The proteins were detected with Luminata Forte Western
188 HRP Substrate (EMD Millipore) or SuperSignal™ West Atto Ultimate Sensitivity Substrate (A38555,
189 Thermo Scientific). Blots were imaged with the Bio-Rad ChemiDoc XRS+ system, and images were
190 processed with the Image Lab software package (Bio-Rad). The primary antibodies and their dilutions
191 were 1:5,000 anti-Pgk1 (ab113687; Abcam), 1:2,000 anti-L-A Gag (obtained from Reed Wickner),
192 1:8000 anti-Hsp60 (received from Toshiya Endo)[46], 1:500 anti-Tom22[46], 1:2000 anti-Om45[46], 1:1000
193 anti-Cox2 (ab110271; Abcam), 1:1000 anti-Sro9, and 1:1000 anti-Slf1 (received from Sandra Wolin)[29].
194
195 **Virus curing.**
196 L-A^0 strains were generated similar to as we described previously[18]. Briefly, a progenitor L-A^0 strain
197 was isolated following treatment with 32 mM Anisomycin (BioShip ANS245) for 4 days in YPD media
198 and plating for single colonies. Isolates were tested for the presence of the L-A genome by RT-PCR.
199 This L-A^0 strain was then used for subsequent backcrossing with *mak3Δ* to generate other L-A^0 strain
200 background.
201
202 To evict L-BC, cells were transformed with the *L-BC GAG (P_{GAL1})* plasmid and grown overnight in –
203 URA drop out media supplemented with 2% raffinose. The saturated culture was diluted and grown in

204 raffinose to log phase before treated with 2% galactose for 24 hours. The resulting culture was plated for
205 single colonies on an agar plate containing synthetic complete media supplemented with 5-FOA. Isolates
206 were tested for the presence of the L-BC genome by RT-PCR.
207
208 **RNA extraction and reverse transcription.**
209 10 OD of log phase cells was harvested and resuspended in phenol solution (P4682; Sigma-Aldrich),
210 SDS, and buffer AE (10 mM Tris·Cl and 0.5 mM EDTA, pH 9.0). Samples were incubated at 65°C for
211 30 minutes, and the phase-separated supernatant was washed with chloroform and precipitated in
212 isopropanol overnight. The precipitate was washed with 70% ethanol and dissolved in water. RNA
213 samples were then purified with the RNeasy Mini Kit (Qiagen). Four micrograms of RNA were reverse-
214 transcribed using random nonamers and Maxima H Minus Reverse Transcriptase (Thermo Fisher). The
215 cDNA product was isolated by alkaline hydrolysis and treated with RNase A.
216
217 **Immunofluorescence.**
218 Log phase cells were fixed with 4% formaldehyde and washed 2 times with 1x phosphate-buffered
219 saline (PBS). Cells were resuspended in sorbitol buffer (1.2 M sorbitol and 20 mM potassium phosphate
220 buffer, pH 7.2) and spheroplated with β-mercaptoethanol (M7522; Sigma-Aldrich) and zymolase at
221 30°C. Spheroplasted cells were added onto polylysine coated slides and incubated with primary antibody
222 1:1000 J2 anti-dsRNA (SCICONS) overnight. The cells were detected with 1:1000 cyanine3 conjugated
223 goat anti-mouse (Jackson ImmunoResearch Laboratories) and stained with DAPI. The images were
224 acquired on the Zeiss Axio Imager Z1 with Volocity and processed with ImageJ.
225
226 **Flow cytometry.**
227 Log phase cells were stained with propidium iodide, fixed with 4% formaldehyde, and washed 3 times
228 with 1x PBS. Fluorescence intensity was measured with Becton Dickinson LSR II flow cytometer and
229 analyzed with Flowing Software. The median GFP intensities of three biological replicates were plotted
230 using R studio ggplot2.
231
232 **High copy suppression screen.**
233 A plasmid library of random genomic inserts in the YEP24 plasmid backbone was transformed into a
234 *nuc1Δ ski3Δ* strain and spread onto -URA agar plate for single colonies[47]. Potential suppressors were
235 obtained by growing at 37°C supplemented with glycerol. To confirm that the suppression was plasmid
236 dependent, the potential suppressors were first grown on agar plate containing 0.1% 5-fluoroorotic acid

237 (5-FOA) for counterselection and then transferred to a fresh agar plate at 37°C supplemented with
238 glycerol. The plasmids of the candidates were isolated and sequenced to identify potential genes
239 responsible for the suppression of L-A pathogenesis when over-expressed. The candidate genes were
240 confirmed by spot analysis using p5476 MOBY plasmids.
241
242 **Quantification and Statistical Analysis.**
243 Data was tested for statistical significance using Excel and plotted with R studio ggplot2. The details of
244 the statistical tests are described in the figure legends.
245
246 **Data and Code Availability.**
247 This study did not generate new data/code.
248
249 **References**
250

251 1. Bernheim, A., and Sorek, R. (2020). The pan-immune system of bacteria: antiviral defence as a
252 community resource. Nat Rev Microbiol *18*, 113-119. 10.1038/s41579-019-0278-2.
253 2. Wickner, R.B., Fujimura, T., and Esteban, R. (2013). Viruses and prions of Saccharomyces
254 cerevisiae. Adv Virus Res *86*, 1-36. 10.1016/B978-0-12-394315-6.00001-5.
255 3. Schmidt, N., Lareau, C.A., Keshishian, H., Ganskih, S., Schneider, C., Hennig, T., Melanson, R.,
256 Werner, S., Wei, Y., Zimmer, M., et al. (2021). The SARS-CoV-2 RNA-protein interactome in
257 infected human cells. Nat Microbiol *6*, 339-353. 10.1038/s41564-020-00846-z.
258 4. Smith, R.W., and Gray, N.K. (2010). Poly(A)-binding protein (PABP): a common viral target.
259 Biochem J *426*, 1-12. 10.1042/BJ20091571.
260 5. Koonin, E.V. (1997). A conserved ancient domain joins the growing superfamily of 3'-5'
261 exonucleases. Curr Biol *7*, R604-606. 10.1016/s0960-9822(06)00311-3.
262 6. Zuo, Y., and Deutscher, M.P. (2001). Exoribonuclease superfamilies: structural analysis and
263 phylogenetic distribution. Nucleic Acids Res *29*, 1017-1026. 10.1093/nar/29.5.1017.
264 7. Szewczyk, M., Malik, D., Borowski, L.S., Czarnomska, S.D., Kotrys, A.V., Klosowska-Kosicka,
265 K., Nowotny, M., and Szczesny, R.J. (2020). Human REXO2 controls short mitochondrial RNAs
266 generated by mtRNA processing and decay machinery to prevent accumulation of double-
267 stranded RNA. Nucleic Acids Res *48*, 5572-5590. 10.1093/nar/gkaa302.
268 8. Grover, R., Burse, S.A., Shankrit, S., Aggarwal, A., Kirty, K., Narta, K., Srivastav, R., Ray,
269 A.K., Malik, G., Vats, A., et al. (2019). Myg1 exonuclease couples the nuclear and mitochondrial
270 translational programs through RNA processing. Nucleic Acids Res *47*, 5852-5866.
271 10.1093/nar/gkz371.
272 9. Brown, J.T., Bai, X., and Johnson, A.W. (2000). The yeast antiviral proteins Ski2p, Ski3p, and
273 Ski8p exist as a complex in vivo. RNA *6*, 449-457.
274 10. Benard, L., Carroll, K., Valle, R.C., Masison, D.C., and Wickner, R.B. (1999). The ski7 antiviral
275 protein is an EF1-alpha homolog that blocks expression of non-Poly(A) mRNA in
276 Saccharomyces cerevisiae. J Virol *73*, 2893-2900. 10.1128/JVI.73.4.2893-2900.1999.

11. Anderson, J.S., and Parker, R.P. (1998). The 3' to 5' degradation of yeast mRNAs is a general mechanism for mRNA turnover that requires the SKI2 DEVH box protein and 3' to 5' exonucleases of the exosome complex. EMBO J *17*, 1497-1506. 10.1093/emboj/17.5.1497.
12. Ball, S.G., Tirtiaux, C., and Wickner, R.B. (1984). Genetic Control of L-a and L-(Bc) Dsrna Copy Number in Killer Systems of SACCHAROMYCES CEREVISIAE. Genetics *107*, 199-217.
13. Rowley, P.A., Ho, B., Bushong, S., Johnson, A., and Sawyer, S.L. (2016). XRN1 Is a Species-Specific Virus Restriction Factor in Yeasts. PLoS Pathog *12*, e1005890. 10.1371/journal.ppat.1005890.
14. Burgess, H.M., and Mohr, I. (2015). Cellular 5'-3' mRNA exonuclease Xrn1 controls double-stranded RNA accumulation and anti-viral responses. Cell Host Microbe *17*, 332-344. 10.1016/j.chom.2015.02.003.
15. Ng, C.S., Kasumba, D.M., Fujita, T., and Luo, H. (2020). Spatio-temporal characterization of the antiviral activity of the XRN1-DCP1/2 aggregation against cytoplasmic RNA viruses to prevent cell death. Cell Death Differ *27*, 2363-2382. 10.1038/s41418-020-0509-0.
16. Eckard, S.C., Rice, G.I., Fabre, A., Badens, C., Gray, E.E., Hartley, J.L., Crow, Y.J., and Stetson, D.B. (2014). The SKIV2L RNA exosome limits activation of the RIG-I-like receptors. Nat Immunol *15*, 839-845. 10.1038/ni.2948.
17. Miyashita, M., Oshiumi, H., Matsumoto, M., and Seya, T. (2011). DDX60, a DEXD/H box helicase, is a novel antiviral factor promoting RIG-I-like receptor-mediated signaling. Mol Cell Biol *31*, 3802-3819. 10.1128/MCB.01368-10.
18. Gao, J., Chau, S., Chowdhury, F., Zhou, T., Hossain, S., McQuibban, G.A., and Meneghini, M.D. (2019). Meiotic viral attenuation through an ancestral apoptotic pathway. Proc Natl Acad Sci U S A *116*, 16454-16462. 10.1073/pnas.1900751116.
19. Li, L.Y., Luo, X., and Wang, X. (2001). Endonuclease G is an apoptotic DNase when released from mitochondria. Nature *412*, 95-99. 10.1038/35083620.
20. Thomson, B.J. (2001). Viruses and apoptosis. Int J Exp Pathol *82*, 65-76. 10.1111/j.1365-2613.2001.iep0082-0065-x.
21. Eastwood, M.D., Cheung, S.W., Lee, K.Y., Moffat, J., and Meneghini, M.D. (2012). Developmentally programmed nuclear destruction during yeast gametogenesis. Dev Cell *23*, 35-44. 10.1016/j.devcel.2012.05.005.
22. Eastwood, M.D., and Meneghini, M.D. (2015). Developmental Coordination of Gamete Differentiation with Programmed Cell Death in Sporulating Yeast. Eukaryot Cell *14*, 858-867. 10.1128/EC.00068-15.
23. Koonin, E.V., and Krupovic, M. (2019). Origin of programmed cell death from antiviral defense? Proc Natl Acad Sci U S A *116*, 16167-16169. 10.1073/pnas.1910303116.
24. Weber, F., Wagner, V., Rasmussen, S.B., Hartmann, R., and Paludan, S.R. (2006). Double-stranded RNA is produced by positive-strand RNA viruses and DNA viruses but not in detectable amounts by negative-strand RNA viruses. J Virol *80*, 5059-5064. 10.1128/JVI.80.10.5059-5064.2006.
25. Welsch, S., Miller, S., Romero-Brey, I., Merz, A., Bleck, C.K., Walther, P., Fuller, S.D., Antony, C., Krijnse-Locker, J., and Bartenschlager, R. (2009). Composition and three-dimensional architecture of the dengue virus replication and assembly sites. Cell Host Microbe *5*, 365-375. 10.1016/j.chom.2009.03.007.
26. Fernandez de Castro, I., Tenorio, R., and Risco, C. (2016). Virus assembly factories in a lipid world. Curr Opin Virol *18*, 20-26. 10.1016/j.coviro.2016.02.009.
27. Liu, Y.X., and Dieckmann, C.L. (1989). Overproduction of yeast viruslike particles by strains deficient in a mitochondrial nuclease. Mol Cell Biol *9*, 3323-3331.

325 28. Johnson, A.W., and Kolodner, R.D. (1995). Synthetic lethality of sep1 (xrn1) ski2 and sep1
326 (xrn1) ski3 mutants of Saccharomyces cerevisiae is independent of killer virus and suggests a
327 general role for these genes in translation control. Mol Cell Biol *15*, 2719-2727.
328 29. Sobel, S.G., and Wolin, S.L. (1999). Two yeast La motif-containing proteins are RNA-binding
329 proteins that associate with polyribosomes. Mol Biol Cell *10*, 3849-3862.
330 10.1091/mbc.10.11.3849.
331 30. Proweller, A., and Butler, J.S. (1996). Ribosomal association of poly(A)-binding protein in
332 poly(A)-deficient Saccharomyces cerevisiae. J Biol Chem *271*, 10859-10865.
333 10.1074/jbc.271.18.10859.
334 31. Brandman, O., Stewart-Ornstein, J., Wong, D., Larson, A., Williams, C.C., Li, G.W., Zhou, S.,
335 King, D., Shen, P.S., Weibezahn, J., et al. (2012). A ribosome-bound quality control complex
336 triggers degradation of nascent peptides and signals translation stress. Cell *151*, 1042-1054.
337 10.1016/j.cell.2012.10.044.
338 32. Anckar, J., and Sistonen, L. (2011). Regulation of HSF1 function in the heat stress response:
339 implications in aging and disease. Annu Rev Biochem *80*, 1089-1115. 10.1146/annurev-
340 biochem-060809-095203.
341 33. Sorger, P.K., and Pelham, H.R. (1987). Purification and characterization of a heat-shock element
342 binding protein from yeast. EMBO J *6*, 3035-3041.
343 34. Li, J., Labbadia, J., and Morimoto, R.I. (2017). Rethinking HSF1 in Stress, Development, and
344 Organismal Health. Trends Cell Biol *27*, 895-905. 10.1016/j.tcb.2017.08.002.
345 35. Stark, C., Breitkreutz, B.J., Reguly, T., Boucher, L., Breitkreutz, A., and Tyers, M. (2006).
346 BioGRID: a general repository for interaction datasets. Nucleic Acids Res *34*, D535-539.
347 10.1093/nar/gkj109.
348 36. Espert, L., Degols, G., Gongora, C., Blondel, D., Williams, B.R., Silverman, R.H., and Mechti,
349 N. (2003). ISG20, a new interferon-induced RNase specific for single-stranded RNA, defines an
350 alternative antiviral pathway against RNA genomic viruses. J Biol Chem *278*, 16151-16158.
351 10.1074/jbc.M209628200.
352 37. Hanekamp, T., and Thorsness, P.E. (1999). YNT20, a bypass suppressor of yme1 yme2, encodes
353 a putative 3'-5' exonuclease localized in mitochondria of Saccharomyces cerevisiae. Curr Genet
354 *34*, 438-448. 10.1007/s002940050418.
355 38. van Hoof, A., Lennertz, P., and Parker, R. (2000). Three conserved members of the RNase D
356 family have unique and overlapping functions in the processing of 5S, 5.8S, U4, U5, RNase
357 MRP and RNase P RNAs in yeast. EMBO J *19*, 1357-1365. 10.1093/emboj/19.6.1357.
358 39. Dwivedi, M., Laddha, N.C., and Begum, R. (2013). Correlation of increased MYG1 expression
359 and its promoter polymorphism with disease progression and higher susceptibility in vitiligo
360 patients. J Dermatol Sci *71*, 195-202. 10.1016/j.jdermsci.2013.04.026.
361 40. Zhuang, T., Yi, X., Chen, J., Kang, P., Chen, X., Chen, J., Cui, T., Chang, Y., Ye, Z., Ni, Q., et
362 al. (2020). Intracellular virus sensor MDA5 exacerbates vitiligo by inducing the secretion of
363 chemokines in keratinocytes under virus invasion. Cell Death Dis *11*, 453. 10.1038/s41419-020-
364 2665-z.
365 41. Kopek, B.G., Perkins, G., Miller, D.J., Ellisman, M.H., and Ahlquist, P. (2007). Three-
366 dimensional analysis of a viral RNA replication complex reveals a virus-induced mini-organelle.
367 PLoS Biol *5*, e220. 10.1371/journal.pbio.0050220.
368 42. West, A.P., Shadel, G.S., and Ghosh, S. (2011). Mitochondria in innate immune responses. Nat
369 Rev Immunol *11*, 389-402. 10.1038/nri2975.
370 43. Sitron, C.S., Park, J.H., Giafaglione, J.M., and Brandman, O. (2020). Aggregation of CAT tails
371 blocks their degradation and causes proteotoxicity in S. cerevisiae. PLoS One *15*, e0227841.
372 10.1371/journal.pone.0227841.

373 44. Magtanong, L., Ho, C.H., Barker, S.L., Jiao, W., Baryshnikova, A., Bahr, S., Smith, A.M.,
374 Heisler, L.E., Choy, J.S., Kuzmin, E., et al. (2011). Dosage suppression genetic interaction
375 networks enhance functional wiring diagrams of the cell. Nat Biotechnol *29*, 505-511.
376 10.1038/nbt.1855.
377 45. Bilanchone, V., Clemens, K., Kaake, R., Dawson, A.R., Matheos, D., Nagashima, K., Sitlani, P.,
378 Patterson, K., Chang, I., Huang, L., and Sandmeyer, S. (2015). Ty3 Retrotransposon Hijacks
379 Mating Yeast RNA Processing Bodies to Infect New Genomes. PLoS Genet *11*, e1005528.
380 10.1371/journal.pgen.1005528.
381 46. Sakaue, H., Shiota, T., Ishizaka, N., Kawano, S., Tamura, Y., Tan, K.S., Imai, K., Motono, C.,
382 Hirokawa, T., Taki, K., et al. (2019). Porin Associates with Tom22 to Regulate the
383 Mitochondrial Protein Gate Assembly. Mol Cell *73*, 1044-1055 e1048.
384 10.1016/j.molcel.2019.01.003.
385 47. Kamada, Y., Fujioka, Y., Suzuki, N.N., Inagaki, F., Wullschleger, S., Loewith, R., Hall, M.N.,
386 and Ohsumi, Y. (2005). Tor2 directly phosphorylates the AGC kinase Ypk2 to regulate actin
387 polarization. Mol Cell Biol *25*, 7239-7248. 10.1128/MCB.25.16.7239-7248.2005.
388

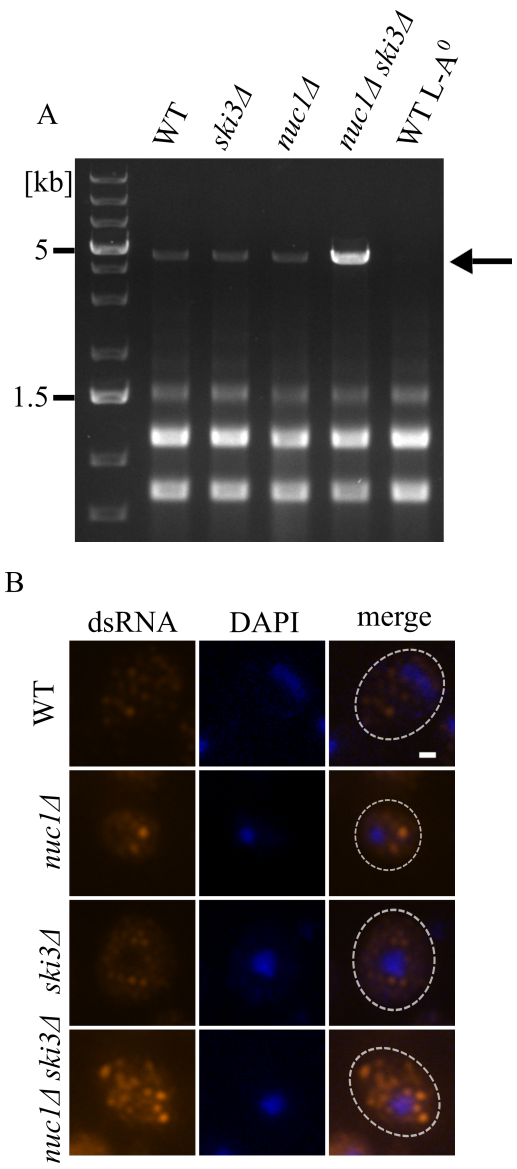

Figure 1. Loss of *NUC1* and *SKI3* displays a synergistic increase in L-A viral load. **(A)** An ethidium bromide-stained gel of total RNA prepared from the indicated strains is shown, with the 4.6 Kb L-A dsRNA band indicated with an arrow. **(B)** Immunofluorescence was used to visualize L-A dsRNA (red) in cells of the indicated genotypes. These strains were cured of the weakly abundant L-BC dsRNA virus to eliminate background staining (see Methods). DAPI staining of DNA is shown in blue. Scale bar, 1 μm.

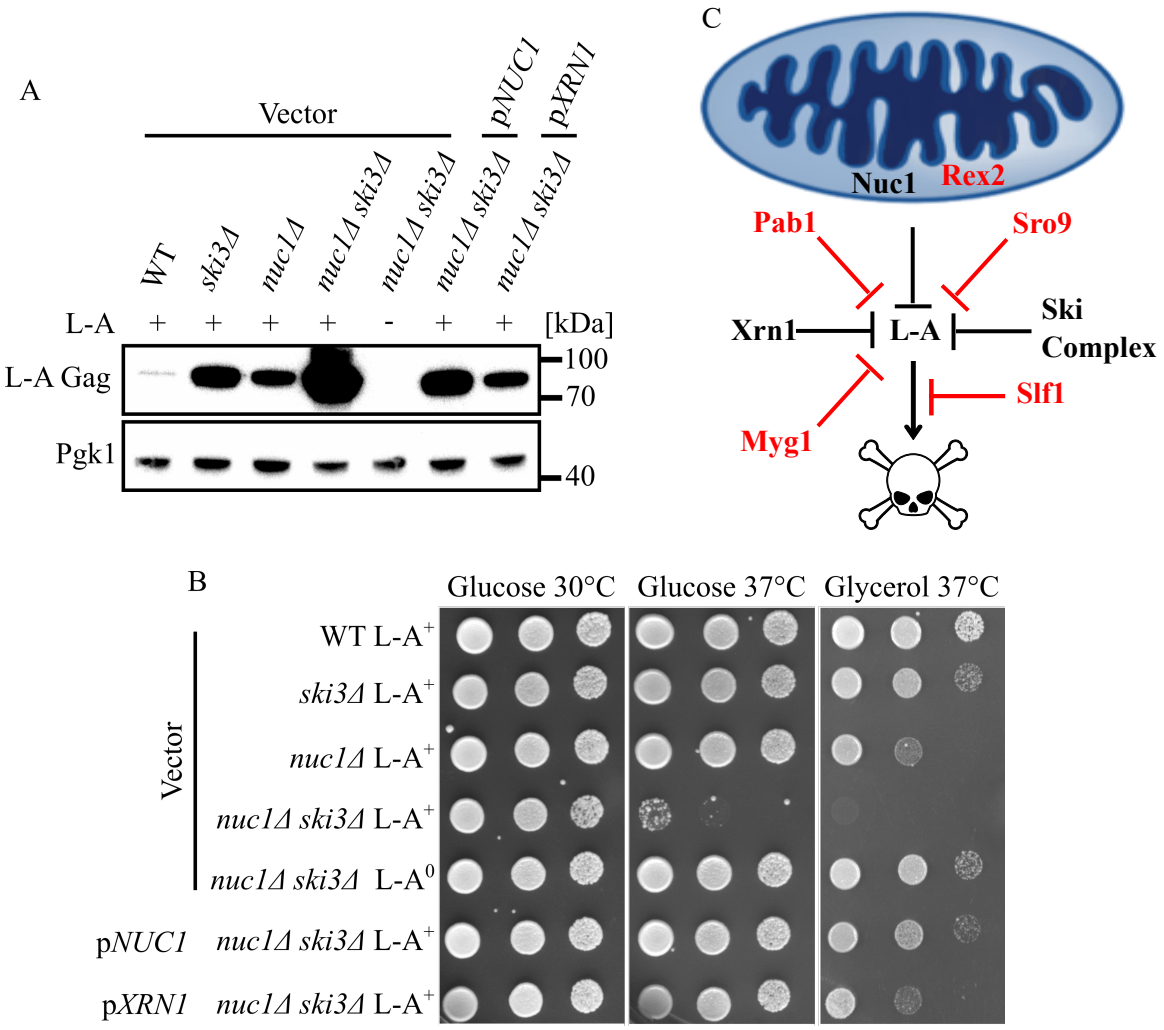

Figure 2. L-A attenuation protects yeast from lethal pathogenesis. **(A)** Western blotting of L-A Gag and Pgk1 protein levels in the indicated strains is shown. Molecular weight markers are indicated on the right. **(B)** Spot test growth assays of the strains from 2A is shown. Strains were spotted on -Leu media containing either glucose or glycerol and grown at the indicated temperatures. **(C)** The mitochondrial proteins Nuc1 and Rex2 collaborate with the cytosolic proteins Xrn1, SkiC, and Myg1 to regulate L-A protein level and ensure cell fitness. The translation control factors Pab1 and Sro9 alleviate L-A pathogenesis by suppressing L-A level while Slf1, the paralog of Sro9, suppress L-A pathogenesis without affecting L-A level. Newly discovered L-A attenuation factors are indicated in red.

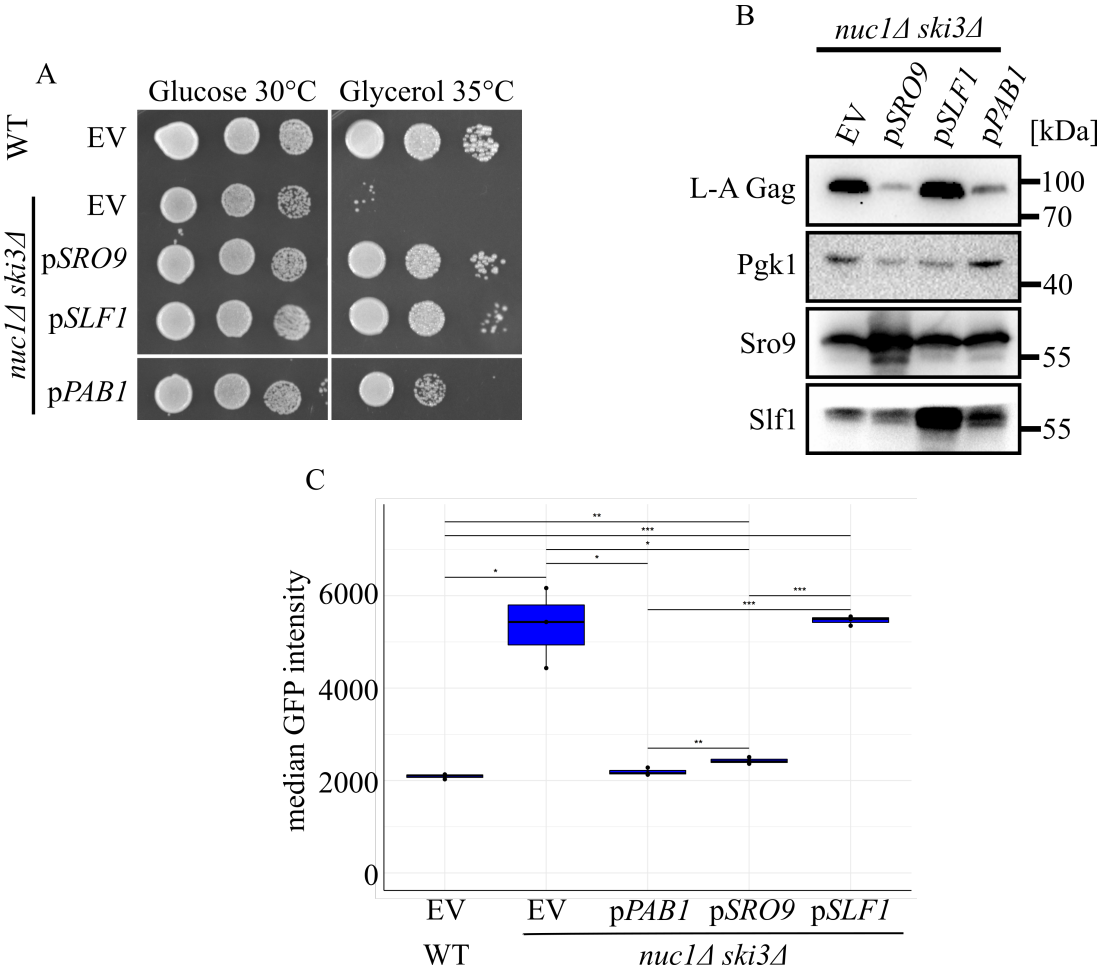

Figure 3. Overexpression of translation control factors alleviate L-A pathogenesis. **(A)** Spot test growth assays of the high copy suppressors *SRO9*, *SLF1*, and *PAB1* are shown. **(B)** Western blotting detection of L-A Gag, Pgk1, Sro9, and Slf1 protein levels in the strains from 3A is shown. Molecular weight markers are indicated on the right. **(C)** Flow cytometry was used to measure HSE-GFP expression in the indicated strains. Median GFP intensity is shown. n = 3. * $p < 0.05$, ** $p < 0.01$, *** $p < 0.001$. The p value was calculated using the unpaired student's t-test.

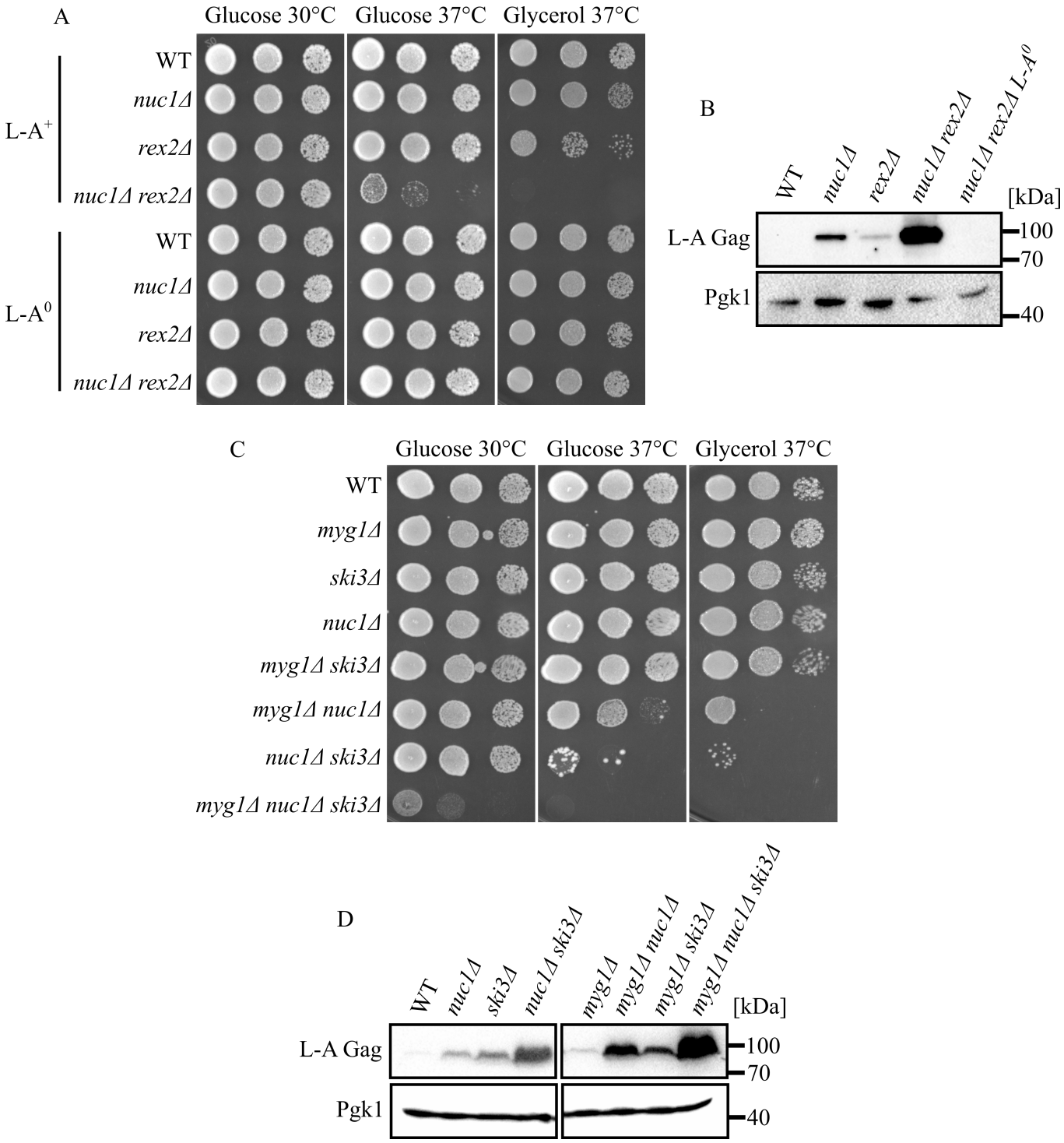

Figure 4. New antiviral factors are identified by exploiting L-A pathogenesis. **(A)** Spot analysis of strains defective in *NUC1* and *REX2* is shown. Strains are spotted on SC media containing either glucose or glycerol and grown at the indicated temperature. **(B)** Western blotting of L-A Gag and Pgk1 protein levels of strains in Figure 4A. Molecular weight markers are indicated on the right. **(C)** Spot analysis of strains defective in *MYG1*, *NUC1*, and *SKI3* is shown. Strains are spotted on SC media containing either glucose or glycerol and grown at the indicated temperature. **(D)** Western blotting detection of L-A Gag and Pgk1 protein levels in the indicated strains is shown. Molecular weight markers are indicated on the right.

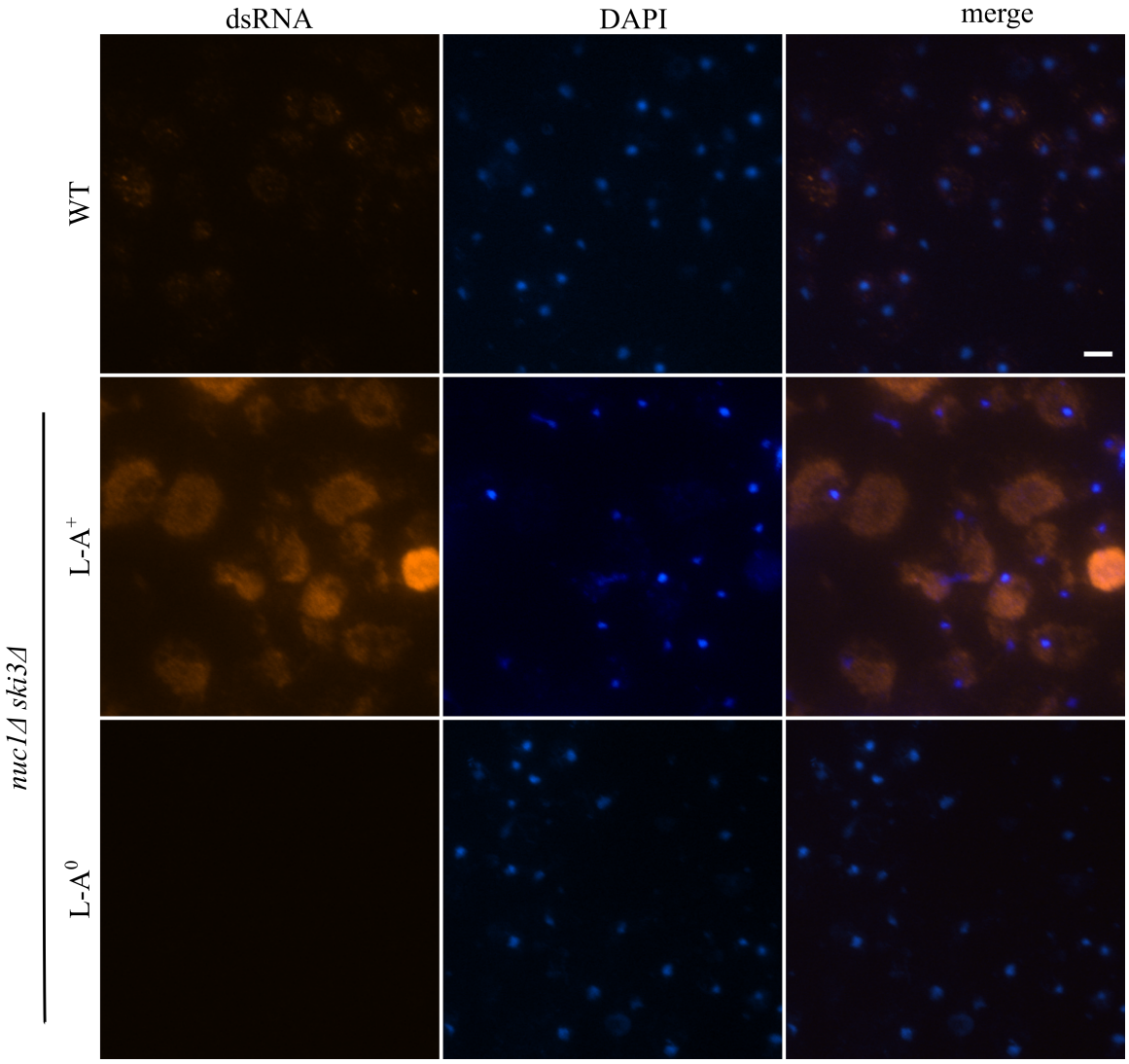

Figure S1. Additional images of immunofluorescence of dsRNA (red) of strains from Figure 1B. Images of fields of cells of indicated genotype is shown. Cells are stained with DAPI to visualize nuclei. Scale bar, 30 μm.

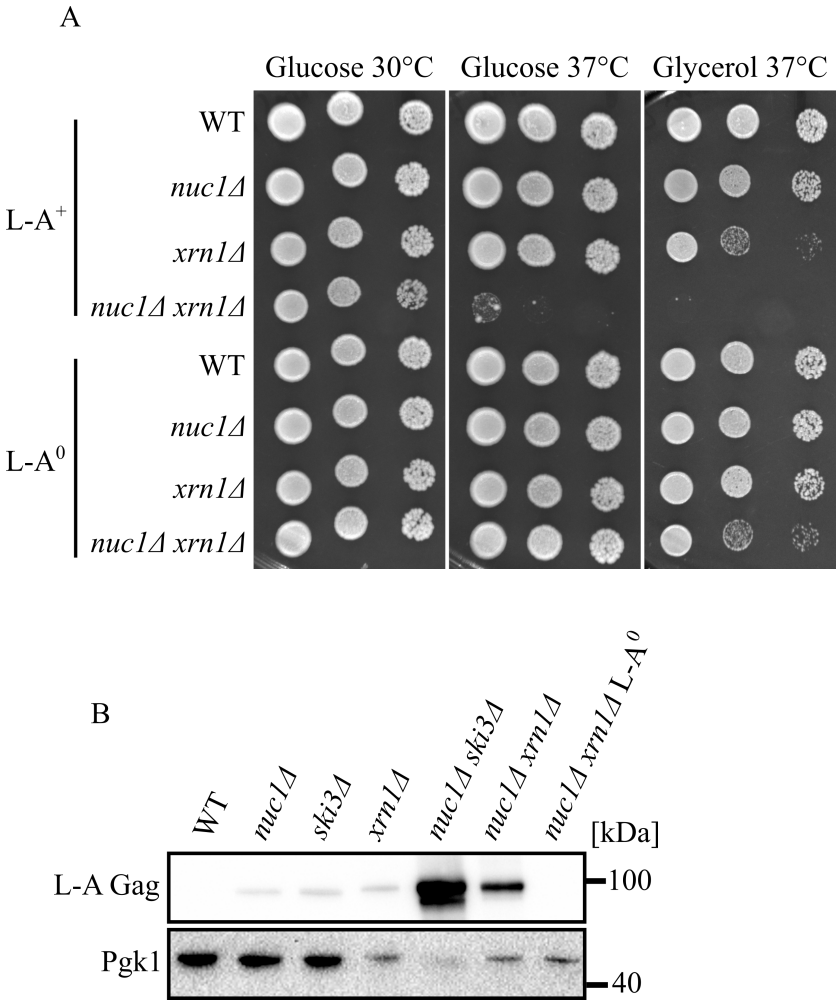

Figure S2. *XRN1*, *NUC1*, and *SKI3* work in parallel pathways to regulate L-A Gag level. **(A)** Spot analysis of strains defective in *NUC1* and *XRN1* is shown. Strains are spotted on SC media containing either glucose or glycerol and grown at the indicated temperature. **(B)** Western blotting of L-A Gag and Pgk1 protein levels of strains in Figure S2A. Molecular weight markers are indicated on the right.

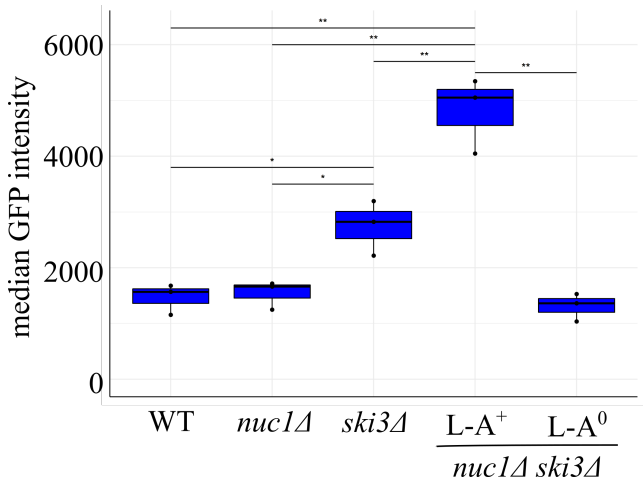

Figure S3. L-A pathogenesis correlates with proteostatic stress. Flow cytometry was used to measure HSE-GFP expression in the indicated strains. Median GFP intensity is shown. n = 3. * $p < 0.05$, ** $p < 0.01$. The p value was calculated using unpaired student's t-test.

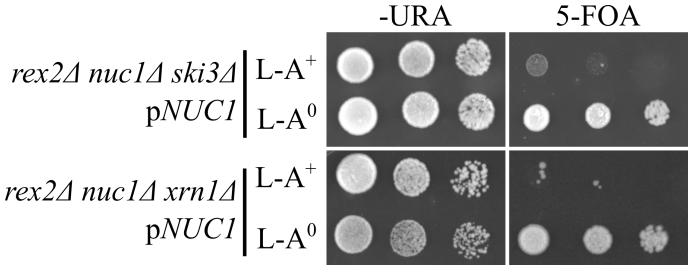

Figure S4. The mitochondrial exonuclease *REX2* is an antiviral factor. Spot analysis of strains defective in 3 parallel antiviral pathways containing plasmid expressing *NUC1* is shown. Strains are spotted on -URA media or synthetic complete (SC) media supplemented with 0.1% 5-fluoroorotic acid (5-FOA).

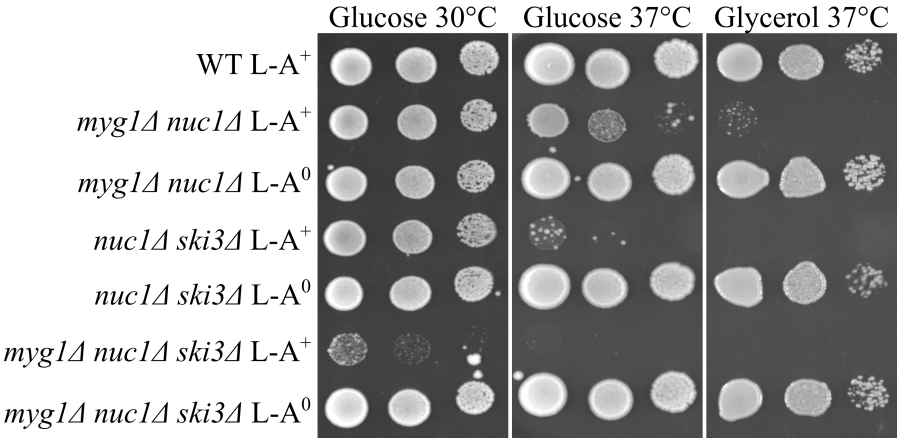

Figure S5. *MYG1* collaborates with *NUC1* and *SKI3* to ensure cell fitness in a L-A dependent manner. Spot analysis of strains defective in *MYG1*, *NUC1*, and *SKI3* with and without L-A is shown. Strains are spotted on SC media containing either glucose or glycerol and grown at the indicated temperature.